C. R. Physique 17 (2016) 294–301

Contents lists available at ScienceDirect

Comptes Rendus Physique

www.sciencedirect.com

Condensed matter physics in the 21st century: The legacy of Jacques Friedel

Friedel oscillations in graphene-based systems probed by Scanning Tunneling Microscopy

Oscillations de Friedel dans les systèmes à base de graphène, sondées par Microscopie à Effet Tunnel

Pierre Mallet [a,b,*], Iván Brihuega [c], Vladimir Cherkez [a,b,d], Jose Marìa Gómez-Rodríguez [c], Jean-Yves Veuillen [a,b]

[a] *Université Grenoble Alpes, Institut Néel, 38042 Grenoble, France*
[b] *CNRS, Institut Néel, 38042 Grenoble, France*
[c] *Departamento de Física de la Materia Condensada, Universidad Autonoma de Madrid, 28049 Madrid, Spain*
[d] *LNCMI, CNRS–UJF–UPS–INSA, 25, rue des Martyrs, 38042 Grenoble, France*

ARTICLE INFO

Article history:
Available online 18 December 2015

Keywords:
Friedel oscillations
Graphene
Dirac fermions
Electronic pseudospin
Scanning tunneling microscopy

Mots-clés :
Oscillations de Friedel
Graphène
Fermions de Dirac
Pseudospin électronique
Microscope à effet tunnel

ABSTRACT

For the last 25 years, scientists have demonstrated the capabilities of Scanning Tunneling Microscopy (STM) to visualize in real space the response of a two-dimensional electron gas to atomic-scale impurities. The analysis of the Friedel oscillations surrounding the impurities yields valuable information regarding the elastic scattering properties, the band structure, the doping level and the symmetry of the electronic states in the two-dimensional host system. We will address in this article the use of this technique for probing the electronic properties of graphene, the star two-dimensional compound of the last decade. In particular, we will emphasize how this technique can be pushed up to unravel the electronic pseudospin, a distinctive degree of freedom of graphene's Dirac fermions.

RÉSUMÉ

Depuis 25 ans, les scientifiques utilisent la microscopie à effet tunnel afin de visualiser dans l'espace direct la réponse d'un gaz d'électron bidimensionnel à des impuretés de taille atomique. L'analyse des oscillations de Friedel générées autour de telles impuretés donne des informations précieuses sur le système 2D : propriétés de diffusion élastique, structure de bande, niveau de dopage et symétrie des états électroniques. Cet article est consacré à l'analyse par microscopie à effet tunnel des oscillations de Friedel dans le graphène, matériau 2D star de cette dernière décennie. En particulier, nous montrons comment cette technique permet d'accéder au pseudospin, un degré de liberté unique propre aux fermions de Dirac du graphène.

* Corresponding author at: CNRS, Institut NÉEL, 38042 Grenoble, France.
E-mail address: pierre.mallet@neel.cnrs.fr (P. Mallet).

http://dx.doi.org/10.1016/j.crhy.2015.12.013
1631-0705/

1. Introduction

Graphene is a unique two-dimensional system regarding its mechanical, optical, thermal and electronic properties [1,2]. Associated with the 2010 Nobel Prize in physics, this material has so many remarkable properties that it is foreseen to be an excellent candidate for future nano-electronics, for instance in devices requiring bendable and transparent conductive electrodes. From a fundamental point of view, graphene has received top billing during the last decade mostly because of its outstanding electronic properties, arising from the massless Dirac nature of its quasiparticles. Such a behavior is the consequence of the honeycomb structure of graphene, made of two equivalent triangular sublattices (labeled A and B sublattices in the following) of carbon atoms, which leads to linear and isotropic low-energy bands at the corners K and K' of the Brillouin zone [3,4].

Another consequence of the bipartite nature of graphene is a peculiar quasiparticle degree of freedom, so-called pseudospin, absent in conventional 2D system. The pseudospin results from the specific symmetry of the quasiparticle wavefunctions $\psi_{\vec{k}}(\vec{r})$ produced by the crystal structure: $\psi_{\vec{k}}(\vec{r})$ has to be a linear combination of two Bloch waves: $\psi_{\vec{k}}(\vec{r}) = C_A(\vec{k})\psi_{\vec{k}}^A(\vec{r}) + C_B(\vec{k})\psi_{\vec{k}}^B(\vec{r})$, where $\psi_{\vec{k}}^A(\vec{r})$ and $\psi_{\vec{k}}^B(\vec{r})$ are built on A and B sublattices respectively. Because A and B are both carbon atoms, the two components $C_A(\vec{k})$ and $C_B(\vec{k})$ are equal in modulus. They are only phase shifted, and the phase relation obtained at low energy, for instance around the K valley, simply reads [4] (a similar expression is found around K' point):

$$C_A(\vec{q}) = \pm C_B(\vec{q})e^{i\theta} \tag{1}$$

where $\vec{q} = \vec{k} - \overrightarrow{\Gamma K}$ is the wavevector measured from the K point, θ is the angle between the $\vec{q}$ vector and the x-axis, and the sign $\pm$ refers to electrons/holes. Written in the $\{\psi_{\vec{k}}^A(\vec{r}), \psi_{\vec{k}}^B(\vec{r})\}$ basis, the wavefunction is thus $\psi_{\vec{k}}(\vec{r}) = \frac{1}{\sqrt{2}}(1, \pm e^{i\theta})$, which defines a pseudospin (in analogy to the real spin of electrons) [5]. Here the pseudospin is intimately tied to the direction of the quasiparticle momentum $\vec{q}$, through the angle θ: the pseudospin is defined parallel (antiparallel) to the momentum for $\psi_{\vec{k}}(\vec{r}) = \frac{1}{\sqrt{2}}(1, +e^{i\theta})$ (for $\psi_{\vec{k}}(\vec{r}) = \frac{1}{\sqrt{2}}(1, -e^{i\theta})$).

Thus, from Eq. (1), electrons and holes with same momentum $\vec{q}$ in the K valley have a pseudospin pointing along the same direction: the pseudospin is parallel to momentum for electrons, and antiparallel to momentum for holes (the situation is reversed at K' point). This allows the introduction of electronic chirality, that is formally a projection of the pseudospin on the direction of motion $\vec{q}$, which is positive and negative for electrons and holes at the K point, respectively [4,5]. The linear band structure and the pseudospin degree of freedom in graphene are the key ingredients responsible for a bunch of phenomena unraveled by magneto-transport experiments: record electronic mobilities at room temperature [6–8], robustness of electronic coherence [9], unconventional quantum hall effect [10,11], weak anti-localization [12–15], and Klein tunneling [5,16,17].

However, all these remarkable electronic and transport properties are subjected to the presence of ubiquitous disorder, which act as scatterers for the Dirac quasiparticles. The impact of point defect impurities upon the local density of states (LDOS) of graphene is a central issue. From a theoretical point of view, as detailed in the first part of this paper, the scattering processes are likely to reflect in LDOS modulations associated with Friedel charge density oscillations generated by the defects, as it is the case in any conventional electron system [18]. But in graphene, the quasiparticle pseudospin plays an important role in the scattering mechanisms, in particular for the backscattering processes [19,20]. Recently, theoretical works based on Green's function formalism have been performed by different groups, in order to compute the graphene LDOS modulations due to a single atomically-sharp impurity [21–26]. Such publications were triggered by the possibility to perform a direct comparison with experimental data obtained by scanning tunneling microscopy (STM), a technique well suited for probing the surface LDOS modulations at the atomic scale [27,28]. In this article, we shall present some key STM results performed on graphene monolayer and bilayer grown on a SiC surface, focusing on the LDOS modulations around impurities. Our approach will mostly be based on the analysis of 2D Fourier transform of the STM data. Following our previous work (Refs. [29,30]), we will especially emphasize how this technique can be pushed up to unravel the electronic pseudospin of the Dirac quasiparticles in graphene. Finally, recent unpublished data obtained on twisted bilayer graphene on Cu(100) will also be discussed.

2. Main text

Scanning Tunneling Microscopy (STM), a technique developed by G. Binnig and H. Rohrer in the eighties [31], is a powerful tool, able to explore the low-energy electronic structure of conductive surfaces with atomic resolution. Nowadays, the contribution of such a technique to nanoscience and surface physics is recognized as colossal and indispensable, especially in the field of conductive two-dimensional (2D) systems lying at metallic or semi-conducting surfaces. Indeed, the tip of the STM is able to measure with high energy resolution (roughly 1 meV at liquid helium temperature) the local density of states (LDOS) of such systems, at the atomic scale. According to Tersoff and Hamann theory [32], the tunneling conductance $dI/dV(\vec{r}, V)$ (with $\vec{r}$ the tip position, V the sample bias and I the measured tunneling current) measured at low temperature and at low bias is proportional to the surface LDOS $\rho_S(\vec{r}, E_F + eV)$ (with E_F the Fermi energy). Depending on the bias sign, the STM is able to probe the surface LDOS for occupied ($V < 0$) or empty ($V > 0$) states. Given the unique lateral resolution of the microscope, STM is the ideal tool for mapping spatial modulations of the LDOS at various energies, such as those associated with Friedel charge oscillations in a conductive 2D system. At that point, it will be helpful for the

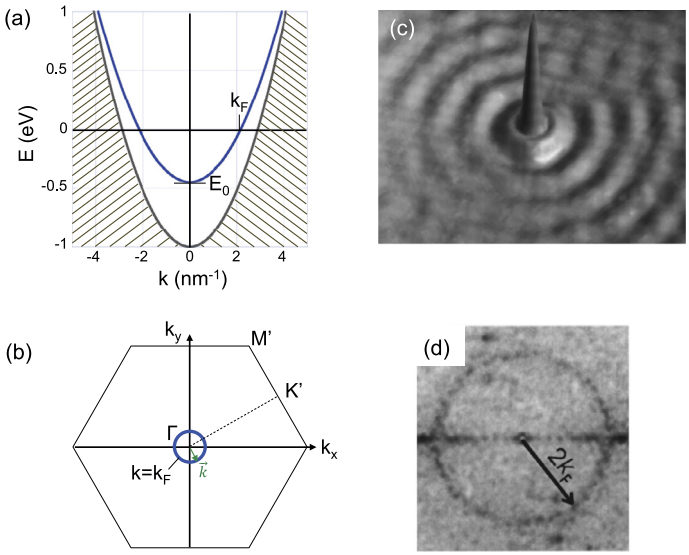

Fig. 1. (a) Schematic of the band structure of the Cu(111) surface (based on angle-resolved photoemission spectroscopy (ARPES) performed by Reinert et al., Ref. [37]). The solid blue curve represents the parabolic and isotropic dispersion of the Shockley surface state, with a band offset $E_F - E_0 \simeq 0.45$ eV, and a Fermi wave-vector $k_F \simeq 2.17$ nm^{-1}. In the presented energy window, the parabolic band lies within a partial bandgap for bulk states (bulk states correspond to striped areas). (b) Fermi surface of the Shockley surface state (central circle) in the first Brillouin zone of Cu(111). (c) Constant current image of one Fe adatom on a Cu(111) surface, demonstrating the capability of STM to image the spatial modulations of the local density of states (LDOS) associated with Friedel oscillations. Image size: 13×13 nm^2, sample bias: 20 mV, $T = 5$ K. This image is extracted from Ref. [36]. (d) Two-dimensional Fourier transform of a 42.5×55 nm^2 STM image of several point defects on Cu(111). Sample bias: 20 mV, $T = 150$ K. Image extracted from [38].

reader to introduce briefly the Friedel oscillations of the charge density, and to clarify the relationship between such charge oscillations and the associated LDOS modulations probed by the STM.

Friedel oscillations of the charge density occur due to the screening by the 2D continuum electrons (or holes) of the local potential associated with any impurity embedded in the system. In his seminal paper published in 1958 [18], J. Friedel calculated the variation of the charge density $\Delta n(\vec{r})$ in a free electron gas due to the screening of an impurity of extra charge Z. He obtained the so-called Friedel rule, which links Z to the phase shifts of the host wavefunctions generated by the impurity. He furthermore calculated the asymptotic form of the charge density $\Delta n(\vec{r})$ far away from the impurity: $\Delta n(r)$ decays as r^{-d} (where r is the distance from the impurity and d is the dimension of the free-electron gas) and oscillates with wavenumber $2k_F$, the diameter of the free-electron-gas Fermi surface. Such oscillations are the so-called Friedel (charge density) oscillations. A textbook presentation of these findings is given in Ref. [33]. Within the Lindhard theory of screening (which holds for weak impurity potentials), this oscillating behavior of the charge density at $2k_F$ is a direct consequence of a singularity of the Lindhard susceptibility at wavevector $2k_F$ [34].

In the following, we focus on Friedel oscillations in conventional 2D systems, which are much more pronounced than in 3D systems because of the $1/r^2$ decay length instead of the $1/r^3$ law [18,35]. As stated above, the STM does not probe directly the Friedel charge oscillations $\Delta n(\vec{r})$, but the LDOS oscillations $\rho_S(\vec{r}, E)$ associated with them. Such LDOS modulations are often labeled the "energy-resolved" Friedel oscillations, since the charge density $\Delta n(\vec{r})$ is calculated by integrating the LDOS over the energies of the occupied states.

The LDOS $\rho_S(\vec{r}, E)$ which is probed by STM at sample bias V (with $E = E_F + eV$) can be written as $\rho_S(\vec{r}, E) = \sum_\alpha \left|\phi_\alpha\left(\vec{r}\right)\right|^2 \delta(E - E_\alpha)$, where the sum is over all states ϕ_α of energy E_α of the 2D system with the impurity. This last expression is worth to be written, since it shows that any impurity-induced spatial modulation of the square-modulus of a given wavefunction will reflect in the LDOS, and thus in the charge density. Within the single particle picture, the LDOS modulation results from quantum interferences generated by elastic scattering of the 2D electron states off the impurity: at a given energy E, a state $\psi_{\vec{k}}\left(\vec{r}\right)$ of the 2D continuum can be scattered into any other state $\psi_{\vec{k}'}\left(\vec{r}\right)$ of the constant energy contour (CEC) at E, giving rise to quantum interferences with dominant wavevector $\vec{k}' - \vec{k}$. For a simple circular CEC, textbook calculations derive the LDOS modulations around the impurity, or so-called Quasiparticle Interferences (QPIs). The QPIs are concentric around the impurity, have a period π/k_E (π/k_F) at energy E (E_F), and decay as $1/r$. Summing over all the occupied states results in the Friedel charge density oscillations, having as said previously a period π/k_F and decaying as $1/r^2$.

As emphasized above, the STM technique is very well suited to detect such QPIs, and appears to be the most direct way to evidence the predicted Friedel oscillations in real space. As an illustration of the conventional 2D case, we show celebrated results obtained in the early 1990s in Donald Eigler's group (IBM Almaden,California) on the Cu(111) surface [36]. This surface and other noble metal surfaces such as Ag or Au(111) hold a Shockley surface state, which was used as a prototype of a nearly 2D free electron gas accessible to the STM tip. The quadratic dispersion associated with the Shockley state lies within a partial bulk gap, allowing an efficient decoupling between the surface and bulk states (Fig. 1a).

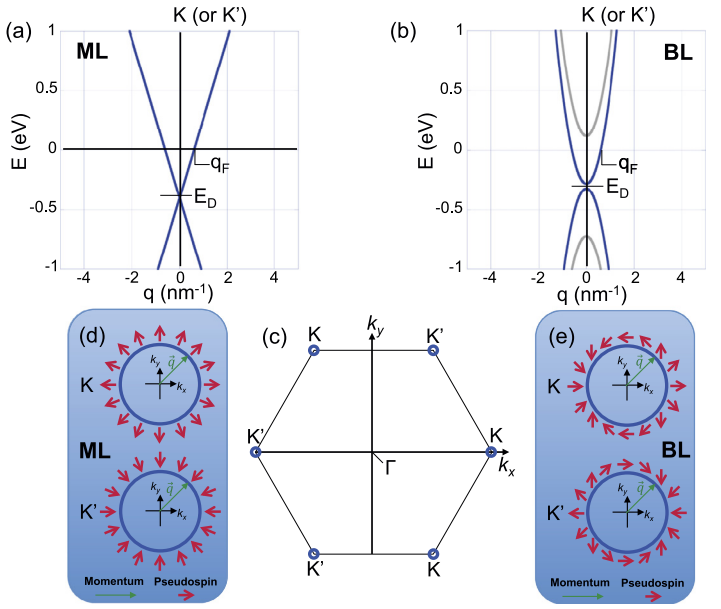

Fig. 2. (a) Schematics of the band structure of monolayer (ML) graphene on SiC(0001) at the K (or K') corners of the Brillouin zone. Two linear and isotropic bands cross at the Dirac point E_D, with $E_F - E_D \simeq 0.4$ eV. (b) Same as (a) but for bilayer (BL) graphene on SiC(0001), with two sets of upside–down parabolic bands, symmetrical to E_D, with $E_F - E_D \simeq 0.3$ eV. Figs. (a) and (b) are constructed from the ARPES data performed by T. Ohta et al., Refs. [53]. (c) Fermi contours of both graphene ML and BL in the first Brillouin zone. (d)–(e) Pseudospin texture (see text) versus momentum direction in the K and K' valleys of graphene, for ML (d) and BL (e).

The bottom of the quadratic band E_0 lies below the Fermi energy ($E_F - E_0 \simeq 0.45$ eV for Cu(111)). At a given energy above E_0, the CEC of the Shockley state is a circle centered at Γ. The Fermi surface (FS) has thus a radius k_F (Fig. 1b), which is the Fermi wavevector of the surface state quasiparticles ($k_F \simeq 2.17$ nm^{-1}). These values of E_0 and k_F are extracted from angle-resolved photoemission spectroscopy published in Ref. [37].

Fig. 1c is a low-bias constant current image from Ref. [36] showing nice circular LDOS fringes around a single Fe adatom deposited on the Cu(111) surface. The period of the QPIs is $\simeq$1.4 nm, which is roughly π/k_F for the Cu(111) surface state. In the presence of a collection of such atomic-point defects, STM images reveal the π/k_F QPIs centered on each defects. Petersen et al. have introduced in 1998 the use of the 2D Fourier Transform (FT) of such STM images to analyze accurately the QPIs [38,39]. An example is given in Fig. 1d, which is the 2D FT of a low-bias STM image of many atomic impurities on Cu(111) [38]. Interestingly, the main signal spots (here in dark) are found on a ring of radius $2k_F$, giving a nice map of the FS. The hereafter $2k_F$ ring in the Fourier transform directly reflects the concentric real space QPIs of wavelength π/k_F. This emphasizes that the LDOS modulations arise mostly from interferences due to backscattering processes (i.e. scattering between states $\psi_{\vec{k}}(\vec{r})$ and $\psi_{-\vec{k}}(\vec{r})$ of opposite momentum on the CEC), which is explained by a maximum joint density of states (JDOS) for these processes. This JDOS argument has been generalized to more complex FS than the one of Cu(111) [40–43]. In a general way, the 2D FT of QPIs compares well not with the FS but with the self-correlation of the FS [44,45]. However, it has been shown that this approach is insufficient in systems with large spin–orbit coupling, for which the wave-function symmetry (for instance the electronic spin) hinders some backscattering processes as on Au(111) or Bi(100) surfaces [46,47].

In the remaining part of the manuscript, we shall concentrate on the STM mapping of the QPIs in graphene, keeping an eye on the trivial case of QPIs in Cu(111) for comparison. Our main goal is to emphasize how the pseudospin degree of freedom of graphene quasiparticles dramatically affects the QPI patterns. To make a clear demonstration, we did some low-temperature STM images on both monolayer (ML) and Bernal stacked bilayer (BL) graphene. In both systems, a pseudospin degree of freedom is defined, but the pseudospin texture is strongly different (see below). From practical considerations, we have used the Si face of commercial 6H-SiC(0001) wafers, which we have graphitized in ultra-high vacuum using surface thermal decomposition at temperatures above 1150 °C [48]. The graphitization is mastered in order to have on the same sample ML and BL graphene areas (i.e. terraces of width 20–100 nm). It is commonly accepted that the graphene layers are separated from the bulk SiC by an interfacial graphitic layer that lacks the graphene π and π^* low-energy electronic bands [49,50]. It results in a quite efficient electronic decoupling of the ML (and BL) graphene from the substrate, yet a substantial n-type doping is found due to charge transfer from the interface.

We start with depicting the low-energy band structure of ML and BL graphene on SiC(0001), as it has been accurately measured by ARPES in Refs. [51–53]. Here and in the following, we intentionally neglect the possible many-body effects (which slightly distort the bands at specific energies) and the trigonal warping arising at high energy. For ML graphene (Fig. 2a), we have two isotropic Dirac cones centered at the corners K and K' points of the Brillouin zone. These cones are

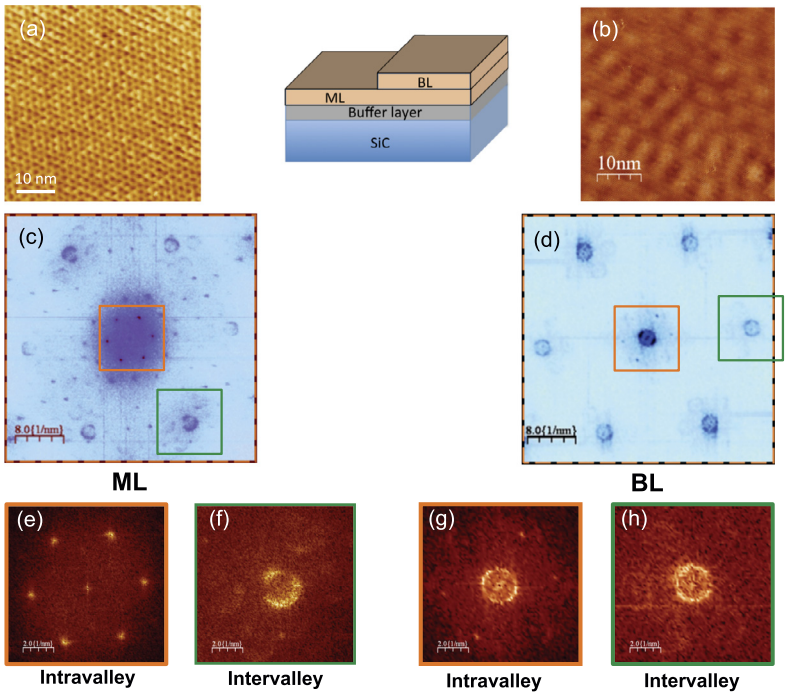

Fig. 3. STM measurements at $T = 5$ K of quasiparticle interferences (QPIs) due to point defects in ML and BL graphene on SiC(0001). Data, originally analyzed using the WSXm software [70], are taken from Ref. [30]. (a) A 50×50 nm^2 constant current STM image on a ML terrace. Sample bias: -4 mV. (b) A 50×50 nm^2 dI/dV STM image on a BL terrace. Sample bias: -25 mV. QPIs of period 5 nm show up on BL (b), but are not detected on ML (a). (c)–(d) Two-dimensional Fourier transform of the STM images shown on (a) and (b). Image sizes: 40×40 nm^{-2}. (e)–(g) Numerical 10×10 nm^{-2} zooms-in of the center of (c) and (d), with an absent (e) or present (g) ring of radius $2q_F$ related to intravalley backscattering processes. (f)–(h) Numerical 10×10 nm^{-2} zooms-in of one of the six outer patterns of (c) and (d), with a split (f) or full (h) ring of radius $2q_F$ related to intervalley scattering processes. The missing intensities (no central ring, split outer rings) found in the 2D FT of the LDOS map of ML graphene originate from the pseudospin texture, as discussed in the main text.

shifted towards negative energy, with a Dirac point E_D around -0.4 eV. This corresponds to a n-type doping of roughly 10^{13} cm^{-2}. The linear bands intercept the Fermi level at $q_F \simeq 0.6$ nm^{-1} (where q_F is the quasiparticle Fermi wavevector measured from the K or K' point). Thus the Fermi surface of ML graphene on SiC(0001) is made of two circles of radius q_F at K and K' points (see Fig. 2c). Importantly, at a given energy $E > E_D$, a state $\psi_{\vec{q}}(\vec{r})$ has a pseudospin parallel (anti-parallel) to the momentum $\vec{q}$ in valley K (K') (see the complete pseudospin texture in Fig. 2d, and note that this texture is reversed for $E < E_D$). Since the pseudospin is locked to the momentum direction, states in a same valley with opposite momentums $+\vec{q}$ and $-\vec{q}$ have opposite pseudospin. A direct consequence is that intravalley backscattering with pseudospin conservation is impossible [19]. This holds for scattering off smooth defects, i.e. with potential variations on a scale larger than the C–C bond length. For comparison, the quadratic dispersion of Bernal bilayer graphene on SiC(0001) is shown in Fig. 2b. The BL is also n-doped, with $E_D = -0.3$ eV, and the wavevector q_F measured from the K or K' point is very close to 0.6 nm^{-1}. Thus the FS of ML and BL graphene on SiC(0001) are mostly similar, and correspond to the schematic in Fig. 2c. However, the pseudospin texture is different between ML and BL: for the latter, states in a single valley with opposite momentums $+\vec{q}$ and $-\vec{q}$ have the same pseudospin orientation (Fig. 2e). BL graphene should hence behave more like a conventional 2D system, with no particular quenching of the backscattering processes on smooth defects.

The experimental STM data taken at 5 K and at small sample bias are presented in Fig. 3. At sufficiently low bias, STM images mostly reflect the LDOS maps at the Fermi energy. Although severals group have undertaken similar experiments to evidence QPIs in graphene on SiC [54–57], no pseudospin-related fine structures in the 2D FT LDOS maps were reported, except by our work [29,30]. Apart from spurious instrumental noise (mechanical vibration, electro-magnetic disturbance, thermal broadening), one has to take care of the lateral size and of the number of pixels in the STM image, which limit the k-space resolution. We performed images as large as 150×150 nm^2 with 4100×4100 pixels, leading to unprecedented high-resolution 2D FT LDOS maps. Figs. 3a and 3b show 50×50 nm^2 STM images of ML (sample bias -4 mV) and BL graphene (sample bias -25 mV) on 6H-SiC(0001). On the STM image of the ML (Fig. 3a), a quasiperiodic triangular array of period 1.9 nm shows up, which arises from the interface reconstruction and is to be distinguished from any QPI pattern. Most evidently, no QPIs with period $\pi/q_F \simeq 5$ nm related to intravalley backscattering are found on this image. On the contrary, the same scale image made on the BL graphene exhibit clear QPIs of period $\simeq$5.2 nm. Given that Fig. 3b is obtained at small sample bias (-25 mV), the QPIs are related without doubt to intravalley backscattering. This striking difference between the two images is highlighted in the 2D FT of Figs. 3a and 3b, respectively shown in Figs. 3c and 3d (for more accuracy, Fig. 3c is in fact obtained from a 100×100 nm^2 STM image of the region shown in Fig. 3a). We

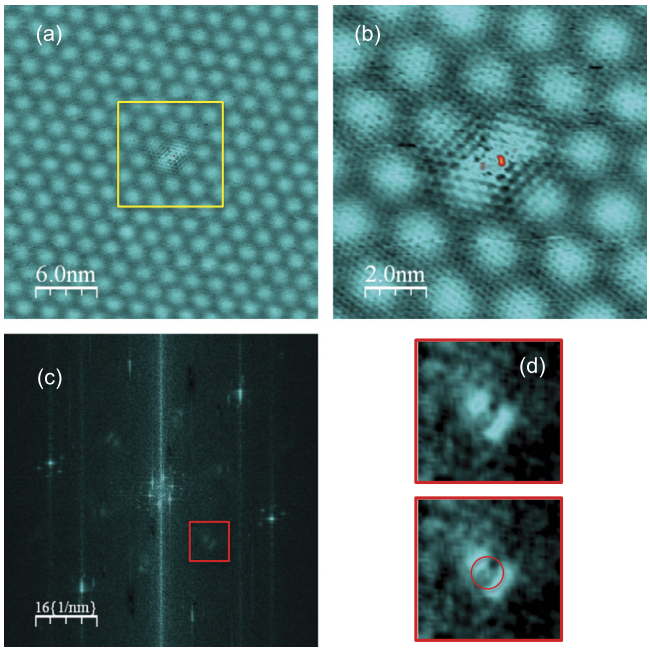

Fig. 4. STM measurements at room temperature of the QPIs induced by one single-point defect on a twisted graphene bilayer grown by chemical vapor deposition on a Cu(100) single-crystal. Data analyzed with WSXm software [70]. (a) Constant current STM image of the twisted bilayer, with an impurity of unknown nature at the center of the image. Image size: 30×30 nm^2, sample bias: -20 mV, current setpoint: 0.2 nA. A moiré triangular superstructure shows up on the whole image, with period 2.2 nm, generated by the 7.0° interlayer twist angle. (b) Numerical zoom-in of the boxed region on (a), showing the $(\sqrt{3} \times \sqrt{3})R30°$ LDOS pattern around the impurity, related to intervalley scattering of the graphene quasiparticles. (c) Two-dimensional Fourier transform of (a), of size 80×80 nm^{-2}. The six inner (outer) bright spots correspond to the moiré pattern (the graphene surface lattice). Six faint contours also show up (one of them is boxed), which are related to intervalley scattering processes (see text). (d) Numerical 10×10 nm^{-2} zoom-in of the boxed region in (c).

first concentrate on the central part of the FT maps, boxed in orange, and zoomed-in in Figs. 3e and 3g. For BL graphene (Fig. 3g), a central ring of radius $2q_F$ is present, corresponding to the FT of the QPIs of period π/q_F shown in Fig. 3b, and thus associated with the intravalley backscattering processes. This result is very similar to the 2D FT LDOS map shown in Fig. 1d for Cu(111). If one turns now to the ML (Fig. 3e), this $2q_F$ ring is missing. The most direct explanation for this different behavior is that the pseudospin degree of freedom of quasiparticles hinders the intravalley backscattering processes in graphene ML, but not in BL (see the different pseudospin textures in Figs. 2d and 2e).

As discussed above, this forbidden intravalley backscattering in ML graphene holds for slowly varying impurity potentials [19]. Our interpretation has to be refined since we have clear evidences that our ML (and BL) graphene hold(s) atomically sharp defects (see below), which can locally break the AB sublattice symmetry and thus restore intravalley backscattering without preserving the pseudospin. However, T-matrix calculations [22–25] have clearly demonstrated that a single atomic sharp impurity located on one single carbon atom of graphene ML induces LDOS modulations of period π/q_F, which are out of phase by a factor π between A and B sublattices. As shown in the calculation, this gives rise to a cancellation of the central ring of radius $2q_F$ in the 2D FT of the LDOS map, corresponding to the smearing out of the π/q_F QPIs in the LDOS. This result is a direct consequence of the wavefunction symmetry (i.e. the pseudospin) in graphene ML. For the BL, similar calculations [22] show that the standard $2q_F$ ring is present in the 2D FT LDOS map. Thus our results shown in Figs. 3e and 3g are in good agreement with such T-matrix calculations, although we have no direct evidence of π-shifted π/q_F QPIs on ML graphene between A and B sublattices, which we believe is very difficult to detect. Actually, whatever the intravalley backscattering is forbidden (case of smooth impurities or defects preserving the AB symmetry) or restored (atomic defect breaking the AB symmetry), no central $2q_F$ ring is expected in the 2D FT of the QPIs on ML graphene, which is a fingerprint of the pseudospin texture in ML.

We turn now to the six outer ring-like features present on the large-scale 2D FT LDOS maps shown in Figs. 3c and 3d (see the green box on each figure). These outer rings demonstrate that we have a certain amount of native atomic size defects in our system. They act as short-range potentials that generate (large wavevector) intervalley scattering, and most importantly for QPIs, intervalley backscattering, i.e. coupling between states $\psi_{\vec{q}}(\vec{r})$ of one valley K with states $\psi_{-\vec{q}}(\vec{r})$ of the second valley K'. Such intervalley backscattering processes explain the 6 ring-like shape contours centered at points distant from the center by $\Gamma K = KK'$. The radius of these rings is once again $2q_F$. STM maps of the QPIs associated with such intervalley scattering have been reported by many groups on graphite/graphene samples [58–60,48,54,29,55,61,62]: they form a local $(\sqrt{3} \times \sqrt{3})R30°$ (R3) superstructure that extends to several nanometers from the defect (an example is given in Figs. 4a–b). Because of its very small period, such R3 superstructures are hardly visible on the large-scale images shown

in Figs. 3a–b, although they are indeed present in the 2D FT maps. Interestingly, we see a marked difference in the $2q_F$ rings associated with intervalley scattering between ML and BL graphene (see the magnified views in Figs. 3f and 3h). The ring is split into two arcs for the ML, highlighting that the QPIs related to intervalley-backscattering processes are hindered in some given directions of the reciprocal space. We have shown using a very simple model that the pseudospin was also responsible for these missing intensities in the intervalley-related rings [30]. Moreover, the T-matrix calculations introduced above in the case of single impurity breaking the sublattice symmetry also find a split structure of the outer rings in the 2D FT calculated LDOS maps [22,25].

In the last part of this paper, we want to emphasize that STM images of QPIs can be undertaken on various other graphene-based systems than graphene on SiC. The 2D FT of measured LDOS maps can give valuable informations on the electronic structure of such systems, the most straightforward being the doping level. As an example, we focus on a twisted graphene bilayer on a Cu(100) surface, grown at Néel Institute (Grenoble, France) using a chemical vapor deposition (CVD) method in a dedicated furnace, and subsequently introduced in our UHV STM set-up. This CVD growth is known to introduce rotational disorder between the first and second graphene layer, forming a so-called twisted BL graphene. This twisted BL is very different from the Bernal BL system, regarding its low-energy electronic properties. In particular, for twist angles $\theta > 4$–5° and for energies close to the Dirac point, the two graphene layers are almost electronically decoupled (at higher energy, the interlayer coupling gives rises to van Hove singularities) [63–67].

We show in Fig. 4a a 30×30 nm^2 STM image measured at room temperature of one single (unknown) point-defect on a twisted BL graphene on Cu(100). The interlayer rotation induces a moiré pattern in the STM image. From geometric considerations, the period 2.2 nm of the moiré corresponds to a twist angle of 7° between the two graphene layers [68,67]. Around the impurity at the center of the image, QPIs forming a R3 pattern show up, related to intervalley backscattering. This R3 pattern is magnified on Fig. 4b, which also shows atomic resolution on the surface graphene layer. The 2D FT of Fig. 4a is shown in Fig. 4c. The sample bias is 20 mV, thus Fig. 4c is mostly a 2D FT map of the LDOS at E_F. One recognizes the 6 outer contours related to intervalley scattering as depicted in Fig. 3c. One of such contour is magnified in Fig. 4d. Most evidently, the contour is split into two parts, suggesting a behavior similar to that of ML graphene on SiC(0001) (Fig. 3f). However, it is too delicate here to extract from the center of Fig. 4c information regarding to intravalley scattering. Further low-temperature FT LDOS images with high k resolution shall be undertaken to shed light on the pseudospin effect on QPIs in twisted BL graphene. Turning back to the intervalley-related outer rings of Fig. 4d, we obtain from the separation between the two arcs $4q_F \simeq 1.96$ nm^{-1}, i.e. $q_F \simeq 0.49$ nm^{-1}. This result nicely demonstrates that even at room temperature, one can extract by STM maps of the QPIs the doping level of the surface graphene plane, which is here 7.6×10^{12} cm^{-2} (see similar room-temperature measurements in Refs. [56,69] for graphene on SiC).

3. Conclusion

In this paper, we have reported a study of the quasiparticle interference (QPI) patterns in epitaxial graphene grown on SiC(0001) by using scanning tunneling microscopy and spectroscopy. This technique was carried out to map the spatial modulations of the local density of states (LDOS) of monolayer (ML) and bilayer (BL) graphene in the presence of native disorder. The LDOS maps reveal QPI patterns, associated with the Friedel oscillations of the charge density surrounding the impurities. Such QPIs, often termed “energy-resolved” Friedel oscillations, were analyzed by performing 2D Fourier transforms of the LDOS maps, a powerful method commonly used for many other 2D electronic systems. We emphasized in this work the specificity of the QPIs in graphene, which, as we showed it experimentally, are strongly impacted by the Dirac quasiparticles symmetry (i.e. the electronic pseudospin). QPIs in Bernal bilayer graphene have a more conventional behavior, and we finish the paper by branching the case of twisted bilayer graphene on a Cu(100) surface, which shall deserve further studies in the future.

Acknowledgements

We thank Dipankar Kalita and Vincent Bouchiat at NEEL Institute for providing us with the CVD-grown graphene on Cu(100) sample. P.M., V.C. and J.-Y. V. acknowledge the European Union FP7 “Graphene Flagship” program (Grant No. 604391) for founding part of this work.

References

[1] A.K. Geim, Science 324 (2009) 1530.
[2] A. Ferrari, et al., Nanoscale 7 (2015) 4598.
[3] P.R. Wallace, Phys. Rev. 71 (1947) 622.
[4] A.H. Castro Neto, F.N.M.R. Peres, K.S. Novoselov, A. Geim, Rev. Mod. 81 (2009) 109.
[5] M.I. Katsnelson, K.S. Novoselov, A.K. Geim, Nat. Phys. 2 (2006) 620.
[6] S.V. Morozov, et al., Phys. Rev. Lett. 100 (2008) 016602.
[7] J.-H. Chen, et al., Nat. Nanotechnol. 3 (2008) 206.
[8] A.S. Mayorov, et al., Nano Lett. 11 (2011) 2396.
[9] K.S. Novoselov, A.K. Geim, S.V. Morozov, D. Jiang, Y. Zhang, S.V. Dubonos, I.V. Grigorieva, A.A. Firsov, Science 306 (2004) 666.
[10] K.S. Novoselov, et al., Nature 438 (2005) 197.
[11] Y.B. Zhang, Y.-W. Tan, H.L. Stormer, P. Kim, Nature 438 (2005) 201.

[12] E. McCann, et al., Phys. Rev. Lett. 97 (2006) 146805.
[13] V.I. Fal'ko, et al., Solid State Commun. 143 (2007) 33.
[14] X. Wu, X. Li, Z. Song, C. Berger, W.A. de Heer, Phys. Rev. Lett. 98 (2007) 136801.
[15] F.V. Tikhonenko, A.A. Kozikov, A.K. Savchenko, R.V. Gorbachev, Phys. Rev. Lett. 103 (2009) 226801.
[16] A.F. Young, Ph. Kim, Nat. Phys. 5 (2009) 222.
[17] N. Stander, B. Huard, D. Goldhaber-Gordon, Phys. Rev. Lett. 102 (2009) 026807.
[18] J. Friedel, Suppl. Nuovo Cim. 2 (1958) 287.
[19] T. Ando, T. Nakanishi, R. Saito, J. Phys. Soc. Jpn. 67 (1998) 1704.
[20] V.V. Cheianov, V.I. Fal'ko, Phys. Rev. Lett. 97 (2006) 226801. In this publication, it is shown that the charge density modulations have a $1/r^3$ decay, accordingly to the $1/r^2$ decay of the LDOS.
[21] E. Mariani, L.I. Glazman, A. Kamenev, F. von Oppen, Phys. Rev. B 76 (2007) 165402.
[22] C. Bena, Phys. Rev. Lett. 100 (2008) 076601.
[23] T. Pereg-Barnea, A.H. MacDonald, Phys. Rev. B 78 (2008) 014201.
[24] C. Bena, Phys. Rev. B 79 (2009) 125427.
[25] N.M.R. Peres, L. Yang, S.W. Tsai, New J. Phys. 11 (2009) 095007.
[26] A. Bacsi, A. Virosztek, Phys. Rev. B 82 (2010) 193405.
[27] M.F. Crommie, C.P. Lutz, D.M. Eigler, Nature 363 (1993) 524.
[28] Y. Hasegawa, Ph. Avouris, Phys. Rev. Lett. 71 (1993) 1071.
[29] I. Brihuega, et al., Phys. Rev. Lett. 101 (2008) 206802.
[30] P. Mallet, et al., Phys. Rev. B 86 (2012) 045444.
[31] G. Binnig, H. Rohrer, Helv. Phys. Acta 55 (1982) 726.
[32] J. Tersoff, D.R. Hamann, Phys. Rev. Lett. 50 (1983) 1998.
[33] J.M. Ziman, Principles of the Theory of Solids, Cambridge University Press, 1972.
[34] N.W. Ashcroft, N. David Mermin, Solid State Physics, HRW International edn., Oxford University Press, Oxford, UK, 1987, chapter 17.
[35] F. Stern, Phys. Rev. Lett. 18 (1967) 546.
[36] M.F. Crommie, C.P. Lutz, D.M. Eigler, Science 262 (1993) 218.
[37] F. Reinert, G. Nicolay, S. Schmidt, D. Ehm, S. Hüfner, Phys. Rev. B 63 (2001) 115415.
[38] L. Petersen, et al., Phys. Rev. B 57 (1998) R6858.
[39] L. Petersen, Ph. Hoffmann, E.W. Plummer, F. Besenbaecher, J. Electron Spectrosc. Relat. Phenom. 109 (2000) 97.
[40] Ph. Hofmann, B.G. Briner, M. Doering, H.-P. Rust, E.W. Plummer, A.M. Bradshaw, Phys. Rev. Lett. 79 (1997) 265.
[41] K. Mc Elroy, et al., Nature 422 (2003) 592.
[42] Q.H. Wang, D.H. Lee, Phys. Rev. B 67 (2003) 020511(R).
[43] F. Vonau, et al., Phys. Rev. Lett. 95 (2005) 176803.
[44] K. Mc Elroy, et al., Phys. Rev. Lett. 96 (2006) 067005.
[45] L. Simon, C. Bena, F. Vonau, M. Cranney, D. Aubel, J. Phys. D, Appl. Phys. 44 (2011) 464010.
[46] L. Petersen, L. Bürgi, H. Brune, F. Besenbacher, K. Kern, Surf. Sci. 443 (1999) 154.
[47] J.I. Pascual, et al., Phys. Rev. Lett. 93 (2004) 196802.
[48] P. Mallet, et al., Phys. Rev. B 76 (2007) 041403(R).
[49] F. Varchon, et al., Phys. Rev. Lett. 99 (2007) 126805.
[50] F. Varchon, P. Mallet, J.Y. Veuillen, L. Magaud, Phys. Rev. B 77 (2008) 235412.
[51] A. Bostwick, T. Ohta, T. Seyller, K. Horn, E. Rotenberg, Nat. Phys. 3 (2007) 36.
[52] S.Y. Zhou, et al., Nat. Mater. 6 (2007) 770.
[53] T. Ohta, et al., Phys. Rev. Lett. 98 (2007) 206802.
[54] G.M. Rutter, J.N. Crain, N.P. Guisinger, T. Li, P.N. First, J.A. Stroscio, Science 317 (2007) 219.
[55] L. Simon, C. Bena, F. Vonau, D. Aubel, H. Nasrallah, M. Habar, J.C. Peruchetti, Eur. Phys. J. B 69 (2009) 351.
[56] H. Yang, A.J. Mayne, M. Boucherit, G. Comtet, G. Dujardin, Nano Lett. 10 (2010) 943.
[57] M. Ye, et al., Eur. Phys. J. B 75 (2010) 31.
[58] H.A. Mizes, J.S. Foster, Science 244 (1989) 559.
[59] P. Ruffieux, O. Gröning, P. Schwaller, L. Schlapbach, P. Gröning, Phys. Rev. Lett. 84 (2000) 4910.
[60] P. Ruffieux, et al., Phys. Rev. B 71 (2005) 153403.
[61] M.M. Ugeda, I. Brihuega, F. Guinea, J.M. Gomez-Rodriguez, Phys. Rev. Lett. 104 (2010) 096804.
[62] M.M. Ugeda, et al., Phys. Rev. Lett. 107 (2011) 116803.
[63] J.M.B. Lopes dos Santos, N.M.R. Peres, A.H. Castro Neto, Phys. Rev. Lett. 99 (2007) 256802.
[64] G. Trambly de Laissardiére, D. Mayou, L. Magaud, Nano Lett. 10 (2010) 804.
[65] M. Sprinkle, et al., Phys. Rev. Lett. 103 (2009) 226803.
[66] G. Li, A. Luican, J.M.B. Lopes dos Santos, A.H. Castro Neto, A. Reina, J. Kong, E.Y. Andrei, Nat. Phys. 6 (2009) 109.
[67] I. Brihuega, et al., Phys. Rev. Lett. 109 (2012) 196802.
[68] F. Varchon, P. Mallet, L. Magaud, J.-Y. Veuillen, Phys. Rev. B 77 (2008) 165415.
[69] A. Mahmood, P. Mallet, J.Y. Veuillen, Nanotechnology 23 (2012) 055706.
[70] I. Horcas, et al., Rev. Sci. Instrum. 78 (2007) 013705.